On the structural variety of alkali hydrogen maleates at high pressure.

*Tomasz Poręba[a,c], Piero Macchi[b], Nicola Casati[c]**

Department of Chemistry and Biochemistry, University of Bern, Freiestrasse 3, 3012 Bern

Department of Chemistry, Materials and Chemical Engineering Polytechnic of Milan, Via Mancinelli 7, 20131 Milano

Laboratory for Synchrotron Radiation – Condensed Matter, Paul Scherrer Institute, 5232 Villigen – PSI

high pressure, molecular crystals, phase transitions, maleate

Abstract

The effect of pressure on the structure of pharmaceutical inactive excipients, such as hydrogen maleates, can provide useful information about their stability in the formulation and overall chemical interactions with active ingredients. Hydrogen maleates with small (lithium, sodium, potassium and ammonium) cations, stable at ambient pressure, are shown to undergo various structural changes upon compression. Depending on the cation size, the nature of its interaction with the anion and hydration, their response to pressure leads to hydrogen bonding rearrangement, phase transitions, increase of the cation coordination number, the

transformation in the anions packing and, eventually, collapse of the crystal structure. Initially symmetric intramolecular hydrogen bonds in hydrogen maleates, localize under pressure on one of the oxygens, leading to a break in crystal symmetry. This proton-transfer points to a pressure-driven change of reactivity in this simple system, which acts as prototype for biologically active enzymatic centres.

Introduction

Maleic acid is considered an inactive ingredient in pharmaceutical formulations, and has been placed on a list of pharmaceutically acceptable acids[1]. As a dicarboxylic acid, it forms two kinds of salts with the pharmaceutical active ingredients: the maleates and the hydrogen maleates (HMAL). The latter is widely used to stabilize complex counterions, including volatile amines, in a wide range of pharmaceuticals, such as antipsychotics[2–4], antihistaminics[5,6], antiemetics[7] and anti-parkinson[8] agents.

Hydrogen maleate anion (HMAL) forms a seven-membered ring through intramolecular hydrogen bond between two carboxylic oxygens. This resonance-assisted hydrogen bond (RAHB) locks the ring in a rigid, planar *cis* conformation, with an estimated stabilization of 21.5(2) kcal/mol [9]. The properties of this particular hydrogen bond has been the subject of extensive research including X-ray[10–15] and neutron[16–18] diffraction, NMR[19], vibrational[20,21] and photoelectron[9] spectroscopies, as well as theoretical investigations[9,22–28]. This relatively simple system is used as a prototype for the hydrogen transfer processes in enzymatic reactions[29–31] and DNA intercalations by *ortho*-hydroxyaryl Schiff bases[32,33]. However, features of this RAHB depend on the environment, including the effect of solvation by polar solvents[34–36].

One way to probe different molecular environments of one species is to study different crystals or co-crystals containing it: these might show already several possible packing arrangements coming from the interplay between all packing forces. RAHBs in HMAL salts show a broad range of asymmetry, depending on the supramolecular environment, such as the nature of the counter ion and/or the presence of co-crystallized solvent molecules[16]. This is also reflected in the different packing modes of HMAL anions (Fig.1). Three main supramolecular conformations occur: the parallel co-planar (**PCP**, blue Fig.1), the anti-periplanar (**APP**, orange Fig.1) and the perpendicular (**PRP**, violet Fig.1). In all of these cases, there are short contacts between carboxylic oxygens involved in the RAHB and the C=C double bond of another HMAL. All conformations cover a broader range of distances between the HMALs center of masses, as the anions can translate or tilt from the idealized contact position.

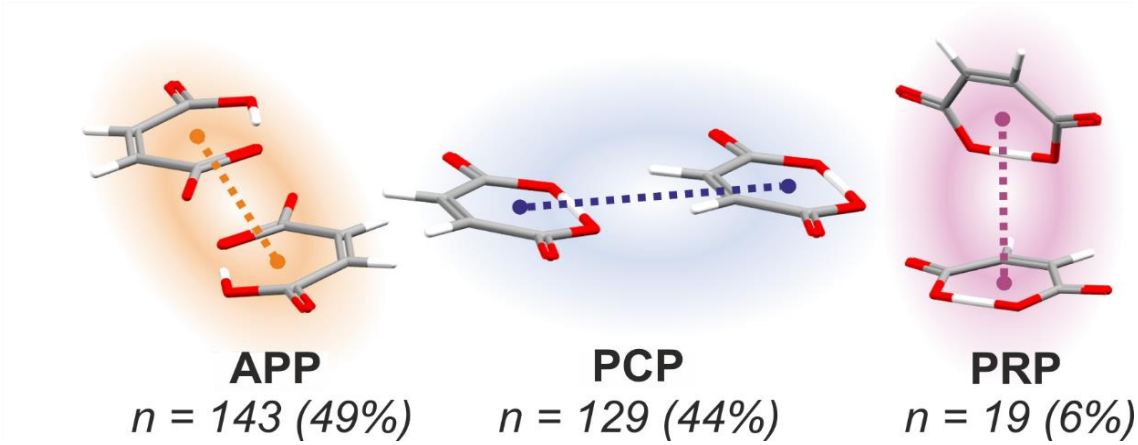

Figure 1.Most common intermolecular conformations of HMALs; n – number of certain type of contacts found in the HMAL structures (208 entries) deposited in CSD v.5.40 (O···C=C distance restrained up to 4 Å). The remaining 1% includes heavily tilted conformations, which cannot be clearly ascribed to one of the categories.

An analysis of the structures deposited in Cambridge Structural Database v.5.40 (CSD)[37] indicates that the parallel co-planar arrangement is the most frequent. Peculiar cases of HMAL anions in perpendicular, PRP conformation include mostly alkali metal and ammonium salts. Interestingly, most of them are isostructural (K, Rb and NH_4 analogues) and contain very short,

symmetric RAHB[11,12,14]. Alkali metals with smaller ionic radii, namely Na^+ and Li^+, form instead PCP arrangements[10,13]. Incidentally, they crystallize as hydrated forms. APP conformation is present in most of the HMALs, allowing for the formation of compact structures, due to the good separation of electrostatically repelling fragments i.e. negatively charged oxygens, which interact with the cations.

A useful approach to gain an insight into the nature of the supramolecular environments is the application of high-pressure (HP) to different crystalline forms of a given molecule. The external force probes the repulsive term of the intermolecular potential, giving a more comprehensive picture of the relative strength of structural motifs. The least compressible contacts are instead those that mostly stabilize a given molecule in the solid state at ambient conditions. In fact, a great variety of crystalline materials show a multitude of structural responses to HP, such as reorganization of hydrogen bonds, changes in conformation, phase transitions, or even chemical reactions[38–43]. Having this in mind, HP can be used as a tool to reshape the HMAL network, including the electronic structure. In alkali metal salts of HMAL, already at ambient pressure, some of the C···O contacts are shorter than a sum of van der Waals radii, at variance from maleic anhydride or maleic acid.

In this work, our aim is a systematic structural investigation at HP on selected alkali metal (Li, Na and K) and ammonium HMAL salts. These compounds include not only different cations but also, as mentioned, different hydrogen bond networks with or without the co-crystallization of water molecules. While the chosen species are chemically similar, they also cover the wide range of supramolecular conformations and intermolecular bonding architecture above described.

Experimental

Material syntheses and crystallization

Lithium hydrogen maleate dihydrate, **LiHMAL**

74 mg (1 mmol) of Li_2CO_3 (>99%, Sigma) was dissolved in 5 ml of ethanol. Subsequently 232mg (2mmol) of maleic acid (>99%, Sigma) was added followed by 1 ml of distilled water. Solution was left for crystallization at room temperature. After three days, transparent needle-like crystals were formed.

Sodium hydrogen maleate trihydrate, **NaHMAL**

106 mg (1 mmol) of Na_2CO_3 (>99.5%, Sigma) was dissolved in 5 ml of ethanol. Subsequently 232mg (2mmol) of maleic acid (>99%, Sigma) was added followed by 1 ml of distilled water. Solution was left for crystallization at room temperature. After one day, transparent plate-like crystals were formed.

Ammonium hydrogen maleate, **NH4HMAL**

96 mg (1 mmol) of $(NH_4)_2CO_3$ (ACS, Reag. Ph Eur., Merck) was dissolved in 5 ml of ethanol. Subsequently 232mg (2mmol) of maleic acid (>99%, Sigma) was added followed by 1 ml of distilled water. Solution was left for crystallization at room temperature. After one day, transparent prismatic crystals were formed.

Potassium hydrogen maleate, **KHMAL**

138 mg (1 mmol) of K_2CO_3 (p.a., Haenseler) was dissolved in 5 ml of ethanol. Subsequently 232mg (2mmol) of maleic acid (>99%, Sigma) was added followed by 1 ml of distilled water. Solution was left for crystallization at room temperature. After two days, transparent prismatic crystals were formed.

Synchrotron single crystal X-ray diffraction experiments

Single crystals of studied compounds were loaded in Merrill- Basset diamond anvil cell (DAC)[44] with 0.5 mm diamond culets. Crystals were placed inside pre-indented steel gaskets with a drilled 250 μm sample chamber. Sizes of the crystals and used pressure-transmitting media[45] are listed in Table 1 SI. Pressure was calibrated in all experiments by ruby

fluorescence[46]. X-ray diffraction experiments were carried out at the Material Science Beamline at Swiss Light Source [47] (details about wavelength are listed in Table 1 SI). For sake of completeness, structures of LiHMAL and NaHMAL were collected additionally in χ =90°position, respectively. CrysAlisPro[48] program suite was used for determination of the UB-matrices and initial data reduction. Reflection files collected at two different χ positions were merged with SORTAV, as implemented in WinGX[49]. Previously unknown structures were solved with Shelxt[50], and subsequently refined with Shelxl[51] as incorporated in OLEX2[52]. Previously reported structures were used as initial models for the HP data refinement[10–13]. All non-hydrogen atoms in NaHMAL, NH4HMAL and KHMAL were refined isotropically. In case of LiHMAL all non-hydrogen atoms were refined anisotropically. Hydrogen atoms were geometrically placed and refined using riding models in all of the structures.

Results

As discussed above, all of the studied compounds contain flat HMAL anions which either form PCP or APP arrangements (Fig.1). LiHMAL and NaHMAL crystallize as hydrates (di- and trihydrate, respectively) and form layers of APP HMAL. The presence of water, and thus intermolecular hydrogen bonds, affects the packing and its behavior at elevated pressure. KHMAL and NH4HMAL crystallize as anhydrous and feature corrugated layers in PRP conformation through O···C=C contacts. Only NH4HMAL features strong intermolecular hydrogen bonds between the ammonium cations and carboxylic oxygens of HMAL.

All of the crystal samples substantially reduced their diffraction quality with increasing pressure. Despite using hydrostatic media with proper chemical (lack of reactivity, poor solvents) and physical (high hydrostatic limits) properties, samples have shown an escalation of crystal mosaicity, a loss of scattering power and a strain-induced peak broadening. In some of the investigated samples, HP caused crystal breaking and amorphization (vide infra).

LiHMAL and NaHMAL

LiHMAL crystallizes in the monoclinic crystallographic group $P2_1/c$. It consists of parallel sheets of HMAL, spaced by $b/2$, linked within the layers by hydrogen bonds from two water molecules (Fig.2). Three water molecules and one carboxylic oxygen from HMAL coordinate the lithium cation. They form a chain of distorted, corner-sharing tetrahedra, which laterally connect HMAL layers. Anions in the layers are arranged in PCP manner, while they form APP contacts between layers (Fig. 2a)

Upon pressurization to 0.97 GPa, LiHMAL undergoes a phase transition to the crystallographic space group $P2_1/m$ (Fig.2b and 4). The process is coupled with the halving of the c axis, which implies a higher symmetry; this is quite uncommon at high pressure where symmetry normally decreases [53,54]. Despite the phase transition, the monoclinic β angle remains rather constant in the entire applied pressure range. A clue of the phase transition can be clearly seen in the evolution of the intermetallic distance (Fig. 3 SI), caused by a complete rearrangement of the lithium coordination sphere: the distorted tetrahedra at ambient pressure turn into face-sharing octahedra at 0.97 GPa, and the distance between two Li atoms decreases sharply by ~0.35Å. This transition is reversible and the $P2_1/c$ polymorph is recovered after pressure release.

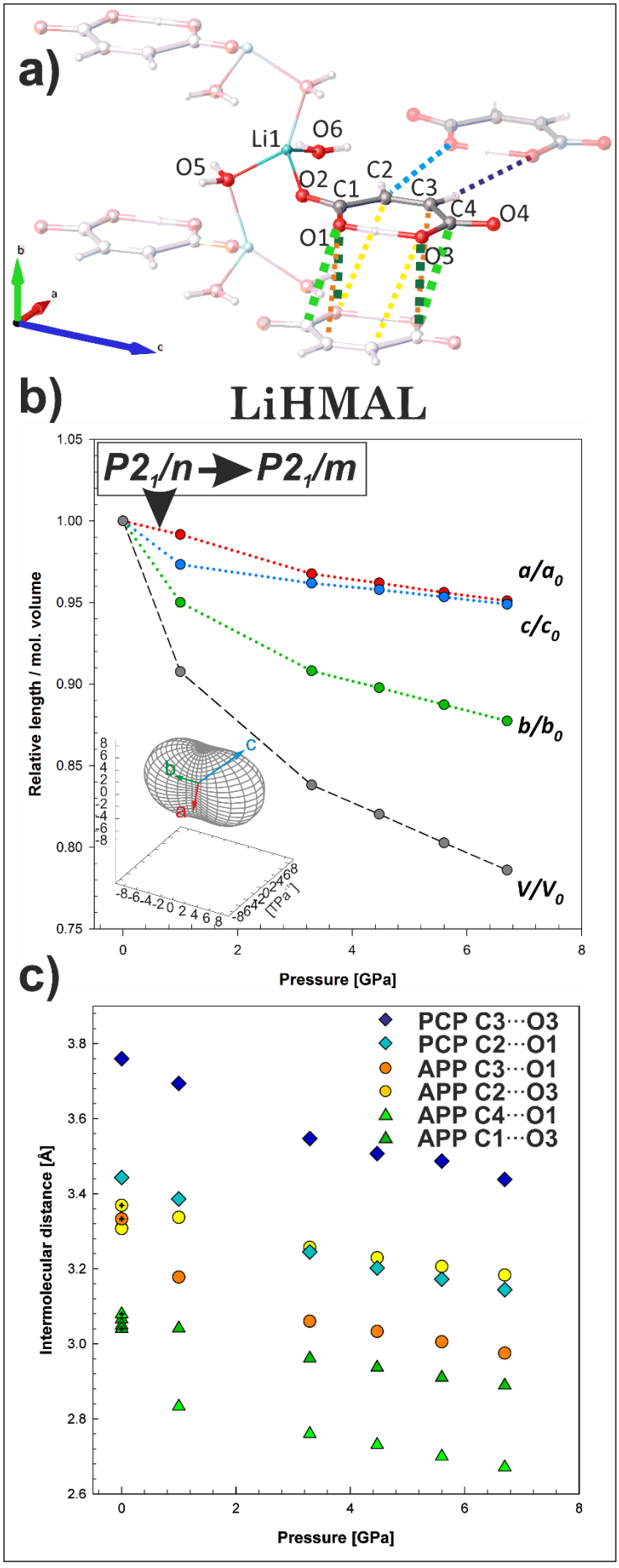
a)
Li1
O6
O5
O2
C1
C2
C3
C4
O4
O1
O3
b
a
c
b)
LiHMAL
P2₁/n → P2₁/m
a/a₀
c/c₀
b/b₀
V/V₀
Relative length / mol. volume
Pressure [GPa]
[Pa]
c)
PCP C3···O3
PCP C2···O1
APP C3···O1
APP C2···O3
APP C4···O1
APP C1···O3
Intermolecular distance [Å]
Pressure [GPa]

Figure 2. a) Molecular structure and atom numbering in LIHMAL. Short C···O contacts are marked with dash b) Evolution of the normalized unit cell axes lengths and molecular volume of LiHMAL under HP. Values of the *c* axis length in LiHMAL HP polymorphs were doubled for clarity. Error bars are smaller than plotted symbols; lines act as a guide for the eye. Inset: compressibility indicatrix relating the principal axes of compression to the crystallographic axes. c) Evolution of APP and PCP C···O intermolecular contacts in LiHMAL (*vide* a)). Points with + represent contacts which undergo symmetrization in HP polymorph.

The Li-O distances within the coordination octahedron shorten linearly after the phase transition with a 0.01Å/GPa^{-1} function. The initial elongation of two Li-O (H_2O) distances upon coordination change from the tetragonal to the octahedral one is in a good agreement with the average values reported in the literature[55]. The final coordination polyhedron around Li is a result of the compromise between the mutual repulsion among the oxygen atoms and the Li-O binding, which is mainly electrostatic in nature. At HP, octahedra are preferred by the system because their geometry allows for a higher maximal density (0.947) compared with tetrahedra (0.822) [56].

Intermolecular distances between the unsaturated carbons of one HMAL and the carboxylic oxygens of the other, experience a continuous compression after the phase transition (Fig.2c). However, this compression affects the APP and PCP contacts with different impact. PCP C2--O1 and C3--O3 contacts (diamonds, Fig 2c) show virtually the same compression rate, which is consistent with compressibility along [100]. Contacts between layers behave quite differently, and show a highly anisotropic behavior. Intermolecular contacts between carboxyl carbons (C1 and C4) and oxygens (O1 and O2) from a neighbor HMAL are the shortest ones, both at ambient and HP (triangles, Fig.2c). This indicates a stronger interaction between electrophilic carbons and nucleophilic, RAHB-engaged oxygens. The compressibility trends of these contacts are virtually the same as the ones to C=C from the respective oxygen atoms.

After the phase transition, compressibility rate of the APP C=C···O contacts is lower than for PCP, as explained above. A calculation of the principal strain axes with PASCal[57] shows that the least compressible direction is approximately [$\bar{1}$0 3] and the most compressible one is [0 1 0] which are the intra- and interlayer directions, as discussed above (see Table 4 SI).

Despite the general structural similarities, the difference between ionic radii of Li and Na causes the shape and connectivity of HMAL layers to differ significantly. In case of LiHMAL, the smaller coordination shell is satisfied by incorporating only three water molecules, while in NaHMAL five molecules are needed. This orders the hydrogen-bonding manner – LiHMAL displays hydrogen bonds only within the HMAL layers, while in NaHMAL they extend beyond them, contributing to the crystal stability in other directions.

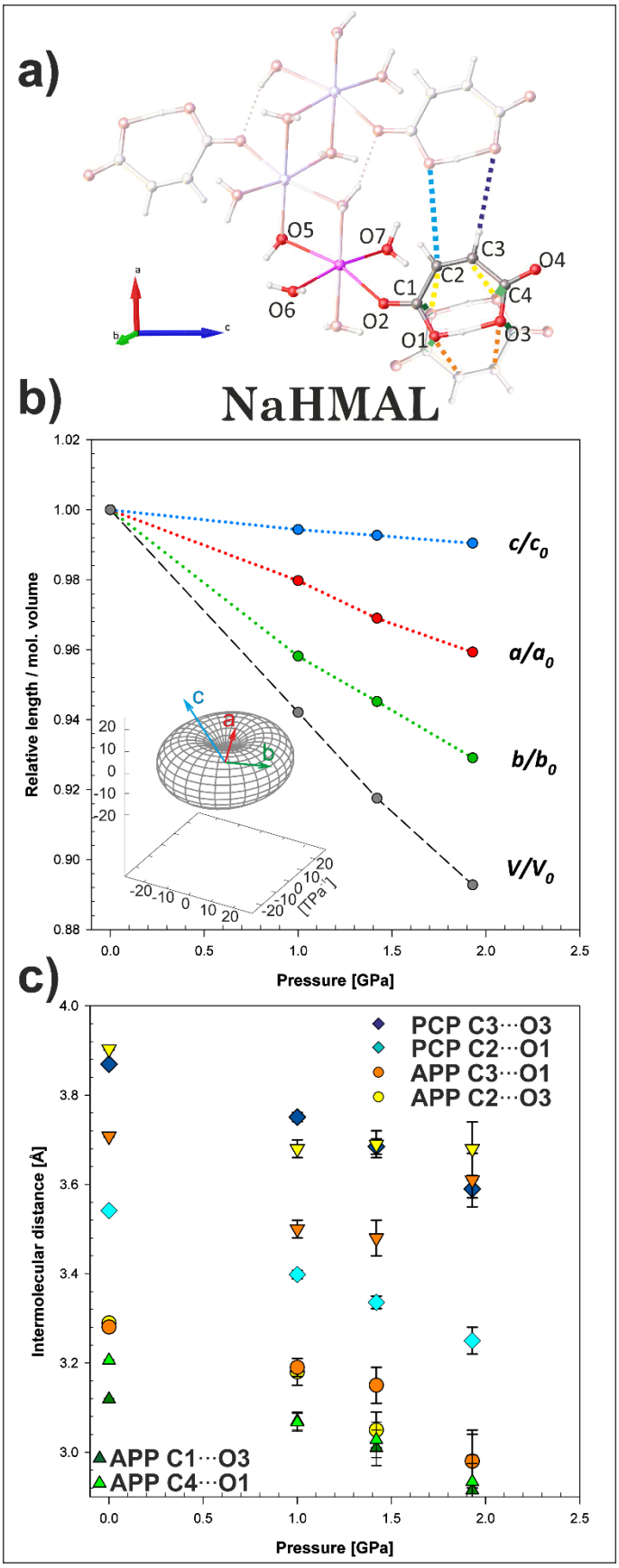
a)
O5
O7
C3
O4
C1
C2
C4
O6
O2
O1
O3
b)
NaHMAL
Relative length / mol. volume
1.02
1.00
0.98
0.96
0.94
0.92
0.90
0.88
c/c0
a/a0
b/b0
V/V0
c
a
b
20
10
0
-10
-20
-20 -10 0 10 20
-20 -10 0 10 20
[TPa]
0.0 0.5 1.0 1.5 2.0 2.5
Pressure [GPa]
c)
Intermolecular distance [Å]
4.0
3.8
3.6
3.4
3.2
3.0
PCP C3···O3
PCP C2···O1
APP C3···O1
APP C2···O3
APP C1···O3
APP C4···O1
0.0 0.5 1.0 1.5 2.0 2.5
Pressure [GPa]

Figure 3. a) Molecular structure and atom numbering in NaHMAL. Short C···O contacts marked with dash b) Evolution of the normalized unit cell axes lengths and molecular volume of NaHMAL under HP. Error bars are smaller than plotted symbols; lines act as a guide for the eye. Inset: compressibility indicatrix relating the principal axes of compression to the crystallographic axes. c) Evolution of APP and PCP C···O intermolecular contacts in NaHMAL (vide a)), reversed triangles represent APP contact between HMAL bilayers (APP C2—O3 and C3--O1 respectively).

NaHMAL crystallizes in the triclinic space group $P\bar{1}$. The structure is composed of the flat HMAL connected through carboxylic oxygen O2 to Na^+ (Fig.3a). As anticipated, sodium is coordinated by five water molecules (two pairs of which are related by an inversion center) forming distorted NaO_6 octahedra, which are edge-connected to each other, extending to a 1D chain along the crystallographic *a* axis. The hydrogen bonding between the bidentate bridging water molecules and the carboxyl groups of different HMALs create a link between the planes (red dashed lines in Fig. 4b). This molecular arrangement results in a set of corrugated HMAL (010) bilayers stabilized alternately by hydrogen bonds and the chains of sodium coordination octahedra (Fig.4b).

A calculation of the principal strain axes with PASCal shows that the least compressible direction is approximately $[\bar{3}\bar{3}\bar{4}]$. The other two directions, which are approximately [0 1 0] and [1 0 0], show similar values (Table 5 SI) and are responsible for most of the compression. They are characterized respectively by weaker PCP and APP contacts between neighbor HMALs. Bifurcated hydrogen bonds from water molecules also have components in these directions.

The single most compressible axis is *b* (Fig.3b), which is characterized by weak APP contacts between HMALs and partially by water hydrogen bonds. Both carboxyl oxygens (O1 and O3)

approach the double-bonded carbons in APP mode at similar rate up to 1.00 GPa (Fig.3c). Eventually, a further pressure increase to 1.93 GPa unusually expands the distance between bilayers, as the in-bilayer counterpart shrinks by virtually the same factor (orange and yellow contacts, Fig.3c). It can be easily tracked as a compression of the contacts between two parallel maleate anions centroids (Fig. 2 SI), where the reciprocity of the contacts evolution is evident.

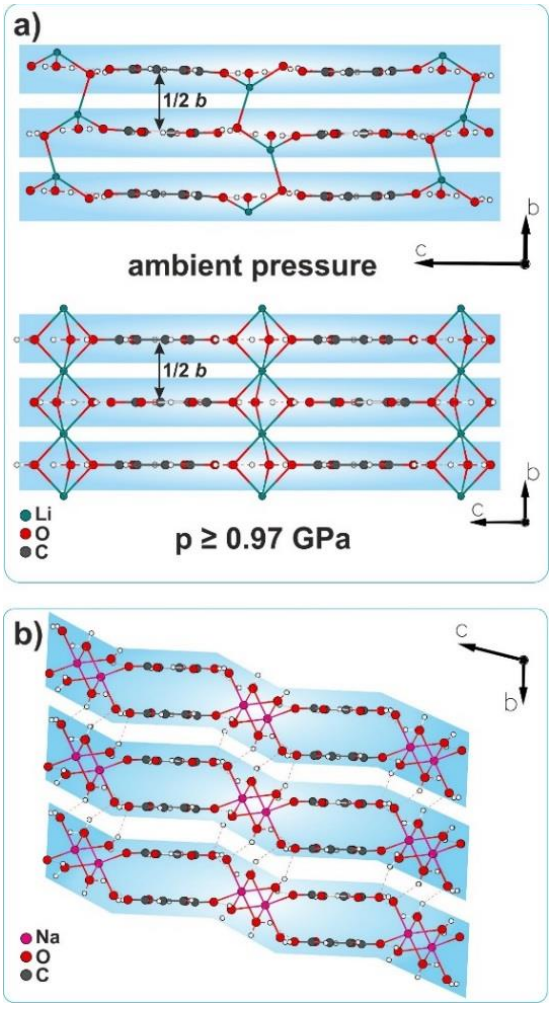

Figure 4. a) Evolution of the structural motif in LiHMAL before and after the phase transition. b) Structural motif in NaHMAL. Layers of HMAL anions are outlined in both structures as blue areas.

Along the *a* axis there is a significant but smaller compression, which reflects the more complex nature of contacts in this direction. On one hand there are the weak C2--01 and C3--03 PCP contacts (Fig.3c), on the other the edge sharing octahedra, which elongate along this axis. While the latter experience a progressive deformation, with the average Na-O distance decreasing and the octahedra distorting from ideal geometry, the former shows a continuous compression (Fig. 3c).

Pressure increase beyond 1.93 GPa leads to the irreversible sample amorphization, which may indicate an abrupt structural change in NaHMAL. The selected crystallographic parameters for LiHMAL and NaHMAL are listed in Table 2 SI.

Structure of NaHMAL, despite the lack of the obvious phase transitions, exhibits a change in hydrogen bonding between carbonyl oxygens of HMAL and water molecules. This is illustrated by the evolution of the HMAL Hirshfeld surface (Fig.4 SI and 5 SI). Hydrogen bonds localize between carbonyl O4 and O3, engaged in RAHB, instead of the direction of C=C bond. APP contacts on one side of the HMAL ring shorten significantly (in bilayer contacts), while they become longer on the other side of the ring (out-of-plane contacts). APP contacts within bilayer seems to engage all of the atoms of a seven-membered HMAL ring, while the ones between bilayers localize on the apical hydrogens and C-O bonds in the vicinity of RAHB.

KHMAL and NH4HMAL

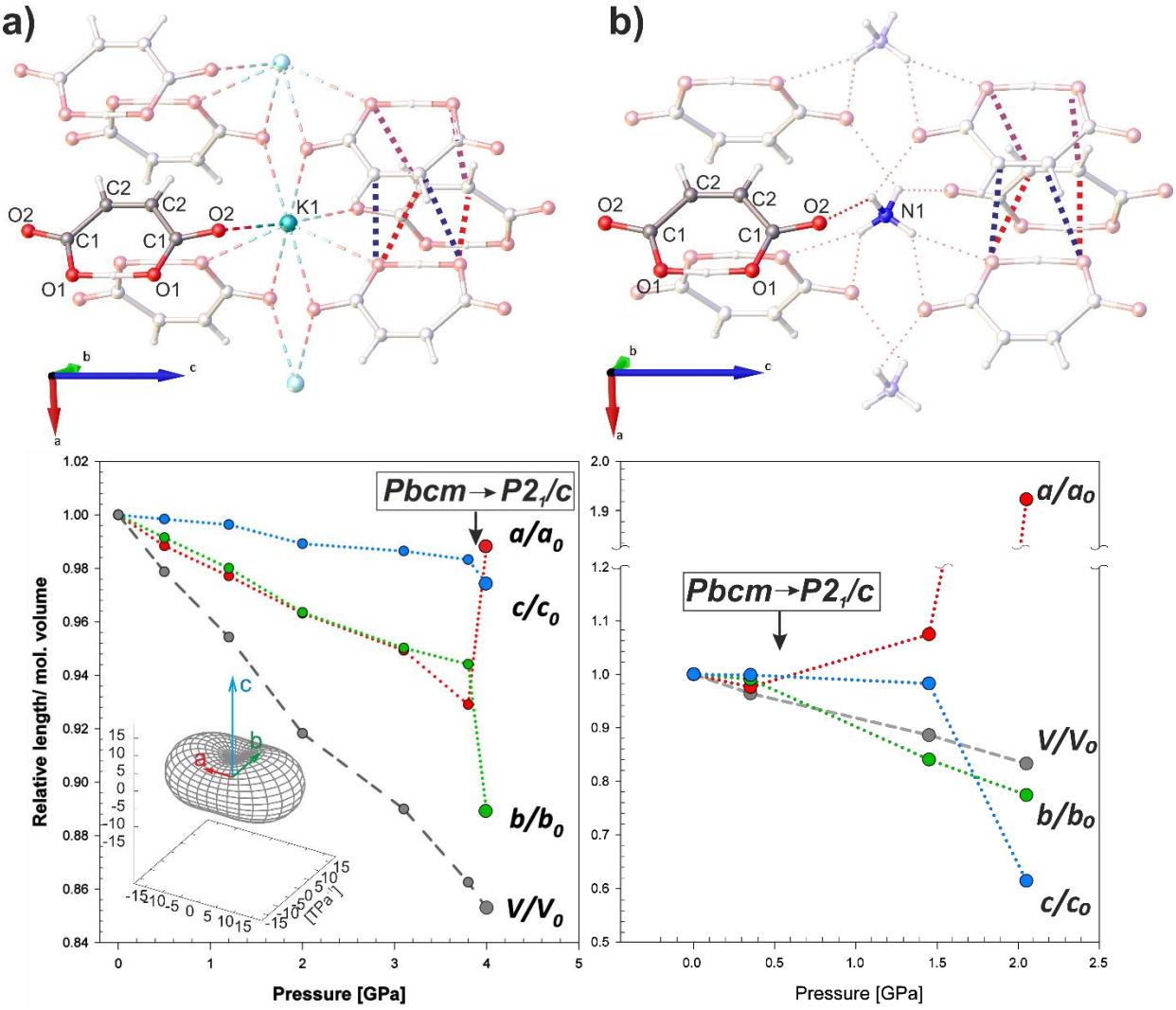

Figure 5. Top: molecular structures and numbering in the a) KHMAL and b) NH4HMAL at ambient conditions. Short C···O contacts marked with dash. Bottom: Linear compressibility and molecular volume change in a) KHMAL and b) NH4HMAL as a function of pressure. Error bars are smaller than the plotted points. Inset: compressibility indicatrix relating the principal axes of compression to the crystallographic axes.

As far as we know, there is only one study of a KHMAL under rather moderate pressure of 4 kbar (0.4 GPa), which does not attribute any visible structural changes to the applied load[58].

KHMAL crystallizes in the orthorhombic space group *Pbcm*. Both apical carbonyl oxygens (O2) in HMAL are surrounded by three potassium cations, which form a regular but not symmetry-constrained triangle (Fig.5a and 6ab), with a mean K-O distance of 2.861Å. Six HMAL molecules coordinate the potassium atoms with their carboxyl groups (Figure 6a). All of them form short contacts through the apical carbonyl groups (O2), of which four lie in an equatorial plane with potassium, and the other two approach the metal apically with an angle of 77° to the equatorial plane, showing at the same time the shortest K-O distance (Fig.6a). Additionally, two of the HMALs lying on the equatorial plane form contacts through the second oxygen, which is involved in the RAHB. However, these are ~0.2Å longer than the ones formed by carbonyl oxygens O2. K atoms therefore have a coordination sphere comprising six short and two longer oxygens and form distorted square antiprisms. They, in turn, form planes of edge-sharing polyhedra perpendicular to the crystallographic *c* axis. These planes are separated by the layers of organic anions, which are linked to each other in PRP fashion. This way, they form a head-to-tail herringbone motif in the (001) plane (Fig.7a). By symmetry, we can distinguish three contacts within the herringbone motif. The shortest one is of PRP type (3.131 Å, red dash Fig.7) connecting two HMALs at 78.4° to one another, and can be viewed as a zigzag sub-motif. The second shortest contact (violet dash, Fig.7) is a laterally-shifted PCP type. Analysis of the structures deposited in CSD, which consist of parallel HMAL assemblies, shows that PCP type of interaction occurs at a different lateral distance between two parallel anions (see Fig.10 and Fig. 1 in SI). The observed range of the lateral spacing is up to circa 3.8Å. In the considered structures, the length of PCP distance between the centers of the HMAL rings spans from 5.9 to 5.0 Å. Below 5.0 Å, instead, the APP conformation is generally preferred. The PCP contact in KHMAL is 4.578 Å, which is in between preferred APP and PCP

conformation (Fig.1 and 10). The third contact is also of PRP type (blue dash, Fig.7a) and is ~0.4 Å longer than the other two contacts.

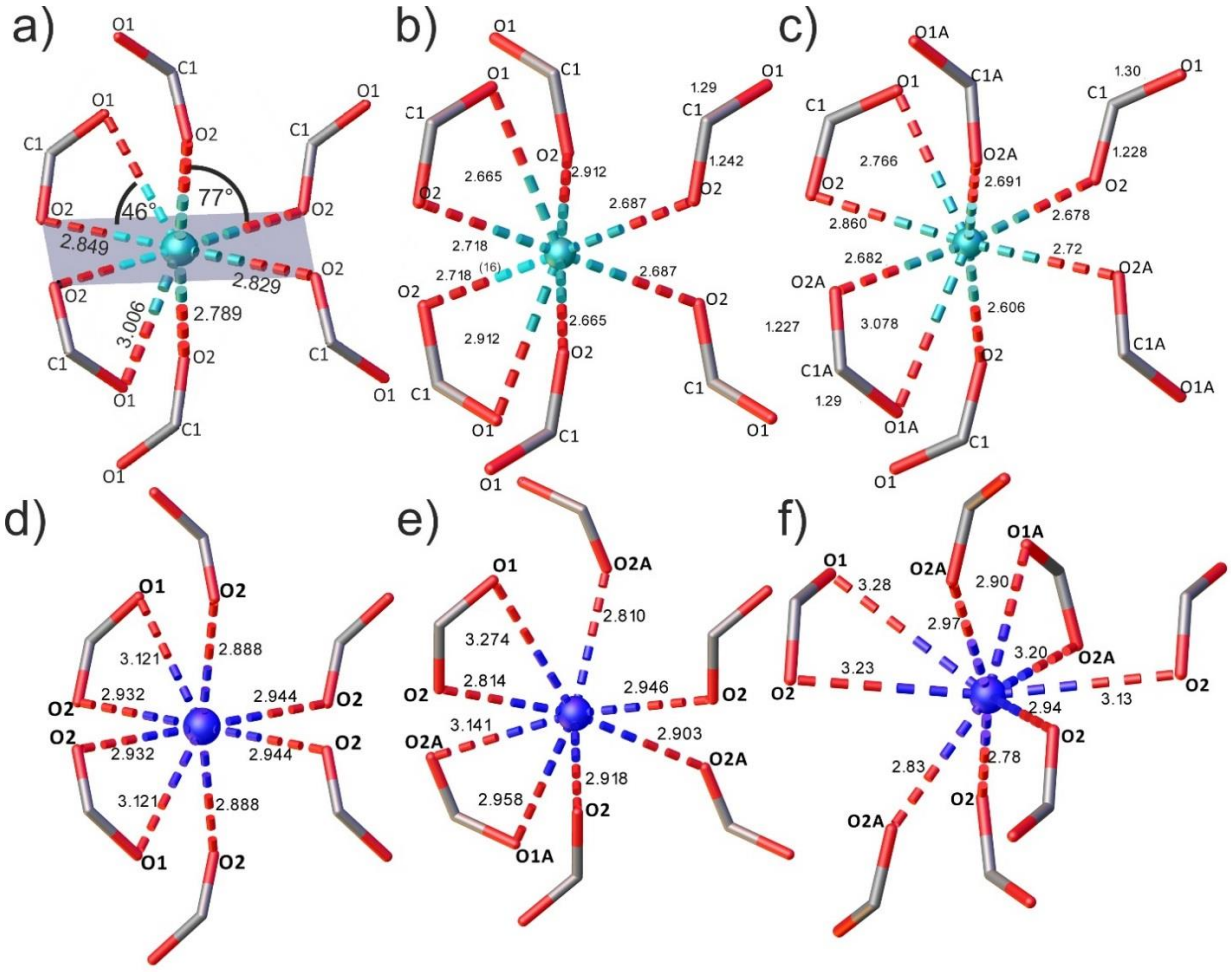

Figure 6. Change in coordination mode in KHMAL between potassium and carboxyl groups at a) ambient pressure, b) 3.77 and c) 4.01 GPa. , and expansion of the ammonium coordination sphere in NH4HMAL at d) 0.33, e) 1.44, fe) 2.06 GPa. Contact lengths are given in [Å], rounded to significant figures.

Following the layered nature of its structure and the presence of soft intermolecular contacts between HMALs, KHMAL shows higher linear compressibility in two axes, namely *a* and *b* (Fig 5a and Table 6 SI). They compress at virtually the same rate and their behavior under HP directly mirrors the compression of the HMAL herringbone motif. On the contrary, the *c* axis is the one along which stronger interactions are observed. As a result, this direction compresses only by 1% up to 3.8 GPa. The coordination polyhedron around potassium, and thus the K-O contacts to HMAL compress continuously up to 3.8 GPa, reaching an average distance of 2.708 Å. Multiple experimental trials showed that KHMAL undergoes an irreversible amorphization above 4.1 GPa. In order to check the pre-amorphized phase, the pressure in the DAC was cautiously increased to 4.01 GPa and the chamber was left to relax any deviatory stresses for a period of 30 days. Pressure determination after this period showed no pressure drop. SCXRD data collected from this sample revealed a second order phase transition to the monoclinic space group $P2_1/c$. The process is coupled with twinning (0.35:0.65 twin ratio). It shows a great distortion in the previous *a* and the *b* directions, which is reflected in the change of the connectivity pattern within the herringbone motif (Fig.7). The phase transition allows HMALs to rotate with respect to each other - the angle between HMAL rings decreases sharply from 79.5 to 70.4°. Initially nearly regular hexagonal (100) net of the potassium atoms undergoes asymmetrization during the phase transition (Fig.8). Only two of the K-K distances shorten significantly. This leads to formation of zigzag chains of KO_6 polyhedral submotif which propagate along the *a* axis (Fig.8c). Intermolecular C···O contacts (Fig. 7b) compress at the similar rate up to the phase-transition pressure. Above 3.8 GPa, asymmetrization of the previously symmetry-related contacts occurs (Fig. 6b). The previously shortest PRP contact (red, Fig.7) elongates and reaches the same length as the PCP one (Fig.7b). Globally, HP forces the system to lower its symmetry, but locally equalizes the PRP and PCP

contacts contributions. Another consequence of a phase transition is a change of potassium coordination mode (Fig.8).

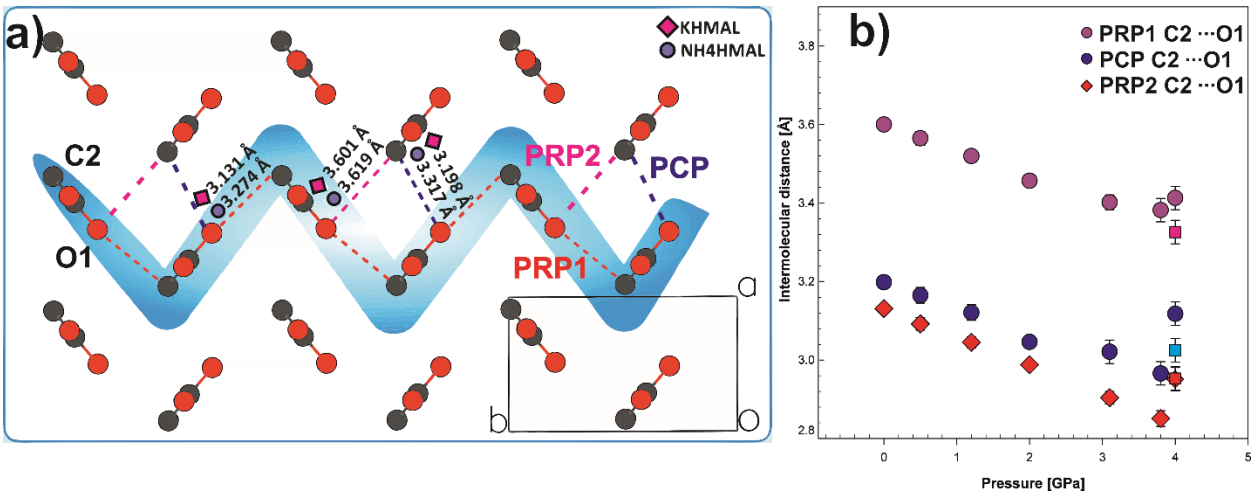

Figure 7. a) Zig-zag HMAL submotif within the herringbone motif in KHMAL and NH4HMAL. C=C ··· O contacts between HMALs marked with dash. Lengths of the contacts at ambient conditions in: □ - KHMAL and ○ -NH4HMAL; b) Intermolecular C--O contacts evolution under HP in KHMAL.

Asymmetrization of the system differentiates the K-O distances with the apical and equatorial carbonyl oxygens (O2 and O2A). Two of the diagonal K-O distances within the equatorial plane elongate, while the other two shorten. One of the contacts between RAHB-involved oxygen (O1) contracts significantly by ~0.15Å while the other one (O1A) elongates by ~0.17Å. This way the coordination mode changes from four monodentate and two loosely bidentate HMALs to five monodentate and one bidentate. While the low-pressure polymorph consists of six short and two long K-O contacts, the HP polymorph has seven short contacts and only one long. The molecular environmental symmetry of HMAL is vital to the degree of localization of RAHB and in KHMAL at ambient conditions, as explained above, the H atom is located at midpoint between the oxygens. While a symmetry break alone does not force the hydrogen to be located at one specific oxygen

atom, study of alkali metal HMALs with asymmetric RAHB show that the hydrogen is always closer to the carboxyl group which interacts via carbonyl oxygen with the cation[16]. Even more, in case when two different metals are involved e.g. potassium and tin (entry GEKFEH in CSD), the hydrogen locates closer to the carboxyl group interacting with the most electronegative metal. It is reasonable to assume therefore that HP-induced localization of carboxyl groups in KHMAL affects not only intermolecular landscape (APP, PCP and PRP contacts, Fig. 10) but also the intramolecular bonding. Although, the data quality was not sufficient to ascertain it experimentally, we can assume that the asymmetrization of RAHB described above occurs at the highest pressure point observed, based on the structural similarities of HP polymorph of KHMAL to the structures described above.

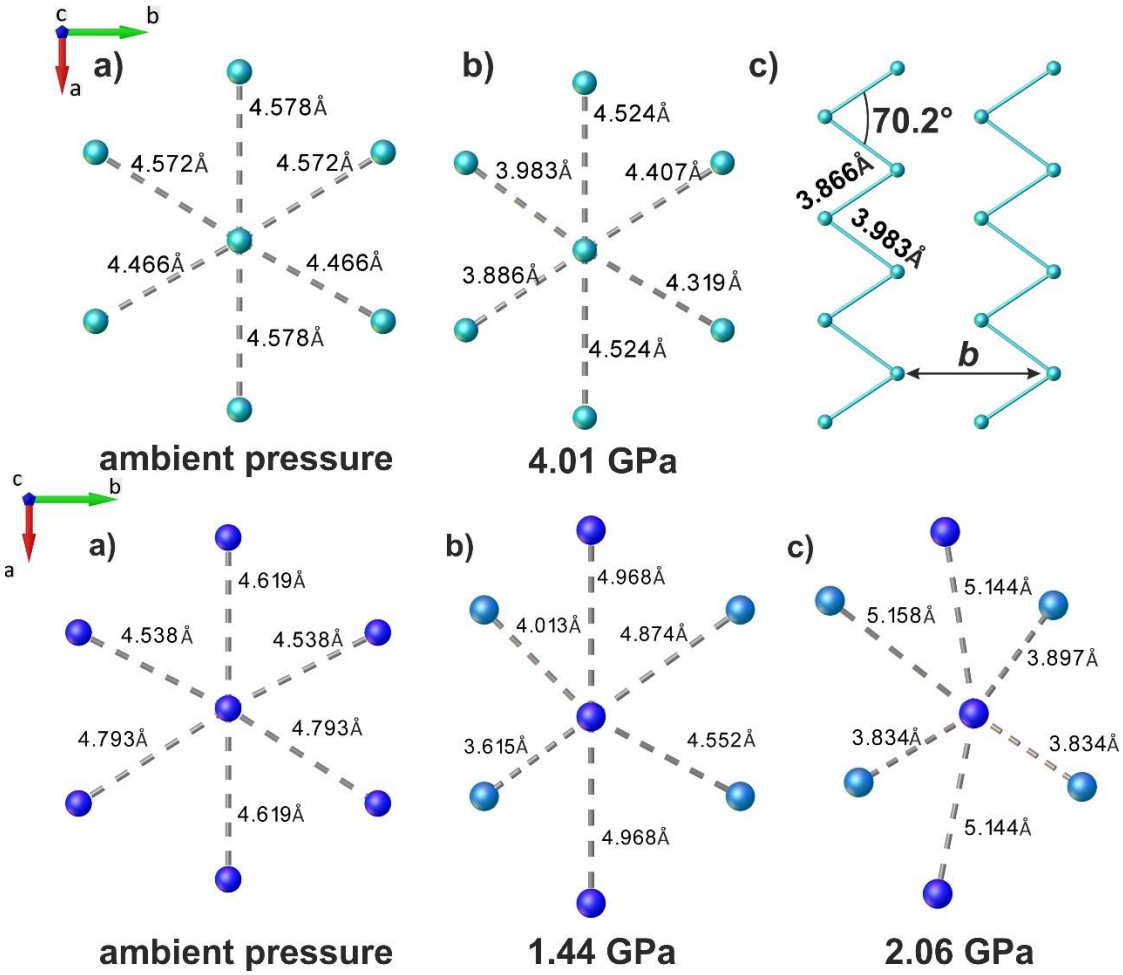

Figure 8. Progressive asymmetrization of the cationic net under HP. Top: potassium atoms positions in 001 layer in KHMAL. Distances between two adjacent atoms at a) ambient pressure, b) 4.01(3) GPa. c) Schematic representation of potassium zig-zag chains at 4.01(3) GPa. Bottom: nitrogen atoms positions in NH4HMAL on (100) plane at ambient pressure (a), 1.44 (b) and 2.06 GPa (c). Light blue spheres represent nitrogen atoms positions shifted along the c axis in respect to the dark blue ones by: b) 0.54, c) 0.94Å.

Despite being isostructural with KHMAL, the volume of the NH4HMAL unit cell is 8% larger (Table 3 SI), due to the longer distances between the carboxyl oxygens and ammonium (3.01Å in average) with respect to potassium (2.86 Å).

As described for KHMAL, the crystal structure is composed of alternating layers of NH_4^+ perpendicular to the *c* axis separated by HMAL. Connectivity of HMALs at ambient pressure resembles the one in KHMAL (Fig.7).

Ammonium cation forms bifurcated hydrogen bonds with four pairs of symmetry-related HMAL oxygens. Two of these pairs of are the apical carbonyl oxygens (O2), while another four contacts are formed with two carboxylic groups, bridging O1 and O2 from both of the molecules. As in the case of KHMAL, oxygens form a distorted square antiprism with the cation, with an average N1-O2 distance of 2.961Å (Fig.8).

At 0.33 GPa, the *b* and *c* axes compress by less than 1% of its initial value (Fig.5b). The *a* axis, however, compresses by 2.5%, which is the direction normal to the zig-zags of the maleic anions. Higher compressibility in this direction stems from the fact that the maleates zig-zag chains are loosely separated by weak PRP And PCP interactions. In the other two crystallographic directions they are more densely packed: in the *b* direction they form short PRP contacts in a zig-zag manner – one HMAL pointing with its carboxyl oxygens towards the double bond of the other HMAL at 83°. Along the *c* direction they form interchanging parallel layers of ammonium cations and HMALs. Contacts between the ammonium cations and oxygens shorten at the similar rate, with an average N1-O2 distance of 2.921 Å.

Pressure of 1.44 GPa greatly changes the structure. Unlike in the case of the lower pressure point, the most affected direction is *b*. In order to achieve the densest packing, the angle within zigzag anion motif decreases greatly from 85 to 51°. It allows chains to fit better to each other in

this direction, satisfying the densest packing. On the contrary, as the zig zag motif turns more acute, it behaves as in 'accordion' fashion – the *a* direction elongates by 10%, while *b* shortens by 15% with respect to lower pressure point (0.33 GPa, Fig.9). Strikingly the PCP contact between HMAL centroids elongates from 4.51 to 4.99Å (Fig.10). This reflects the situation, where decreasing spacing between parallel HMALs forces the increase of the lateral shift between them. Given distance at 1.44 GPa corresponds to the situation in between preferred APP and PCP conformation (Fig. 1.SI).

Pressure-induced distortion forces nitrogen atoms as well as HMALs out of the special positions (Fig.8). As a result, the structure undergoes a phase transition from orthorhombic to the monoclinic $P2_1/c$ group, and the investigated single crystal turns into two merohedral twins with 1:1 ratio. HMALs are not anymore symmetrical at this point, neither are they mirror-plane related in the *a* direction, which allows them to rotate slightly, making the intermolecular contacts between them uneven. Changes in a polyhedron around the ammonium mirror the situation in KHMAL upon the phase transition at 4.01GPa (Fig.8). In addition, in this case, one of the O1A-N1 contact shortens by ~0.16Å, while the other O1-N1 elongates by ~0.15Å. This leads to the change in the coordination mode of ammonium, similar to the one described for the potassium analogue.

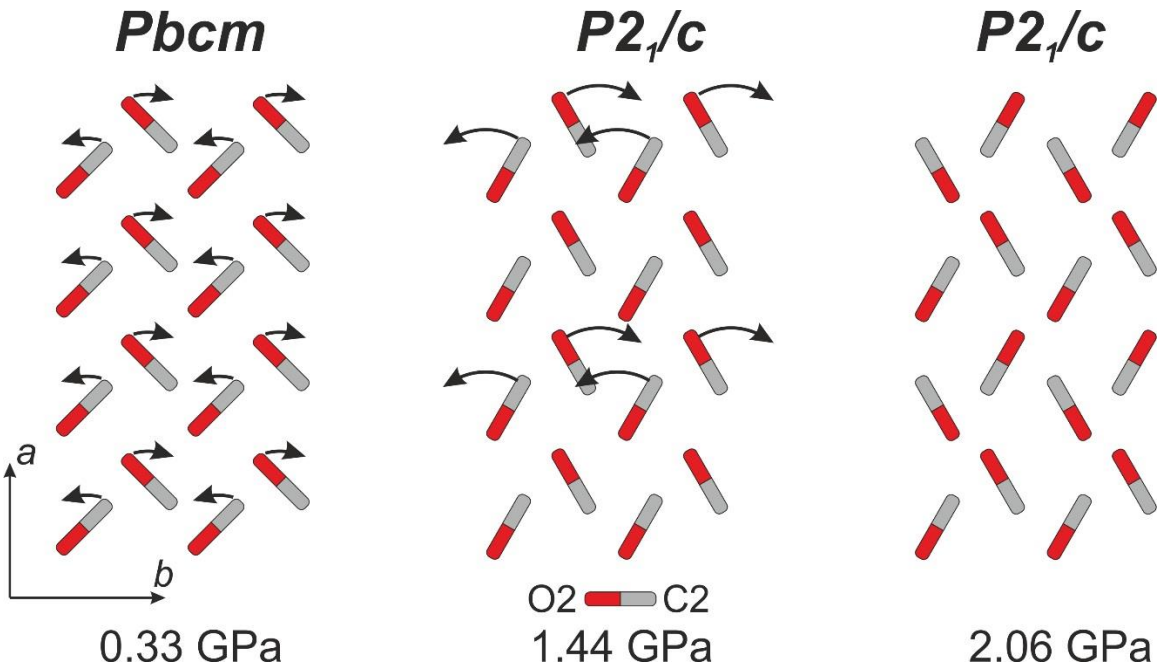

Figure 9. Complex reorganization of HMALs in NH4HMAL under HP. Bicolored bars represent a side view of HMAL. Arrows indicate schematically movement of the anions in order to achieve the higher-pressure structure.

At 2.06 GPa the structure undergoes an isomorphous phase transition (Fig.9) accompanied by a dramatic distortion of the crystal structure (Fig.5b). The massive increase of the β angle from 96 to 146 degrees (in the standard $P2_1/c$ setting) results in almost doubling of the *a* axis. In order to decrease correlation between parameters with respect to the crystallographic *a* and *b* axes, the less oblique cell was chosen, with β = 116°. This required a change in the space group setting from $P2_1/c$ to $P2_1/n$. However, the unit cell distortion does not exclusively explain the unusual elongation of the *a* axis. The herringbone motif collapses, and HMALs assume a different packing (Fig. 10). At this point, in fact, a peculiar change in conformation occurs. Tilting of several HMAL units turn PCP contacts into APP type (Fig. 10). This different type of contact ensures closest packing because of the shorter intermolecular distances and, as the analysis of CSD shows, it

exhibits shorter HMAL-HMAL distances (Fig.1.SI). The coordination sphere of the ammonium cation increases further from 8 to 9, incorporating the additional carbonyl oxygen O2 (Fig.6e). The system achieves closer packing at the cost of bonding expansion. Not only HMALs twist from their starting positions at HP. Initially regular, hexagonal net of NH_4^+ in (001) deforms progressively as the pressure is applied. Comparison with KHMAL shows much higher flexibility of the ammonium net upon pressurization (Fig.8). Although at 1.44 GPa it resembles the trend of shortening of two cation-cation contacts, present in KHMAL at 4.01 GPa, the further pressure increase induces a complete reorganization of the lower pressure motif. Lateral shifts of NH_4^+ positions in the highest-pressure polymorph explain the dramatic elongation of the *a* axis. Correcting for the β angle increase, we can see that $9.035 \cdot \sin(146°) = 5.052$Å, which still corresponds to a minor elongation due to the electrostatic repulsion between HMALs. (Fig.5b).

Pressurization to 2.06 GPa, further shortens the distance between the HMAL and cation on one side of the molecule only, leaving the other one more loosely connected. At the same time the molecules experience new short contacts around C=C, because of the APP intermolecular conformation. These newly formed APP contacts appear on a Hirshfeld surface (Fig. 4 SI) as diffused areas around the HMAL ring and show more even distribution of the short distances around the anions. Further increase in pressure led, as in case of KHMAL, to sample amorphization.

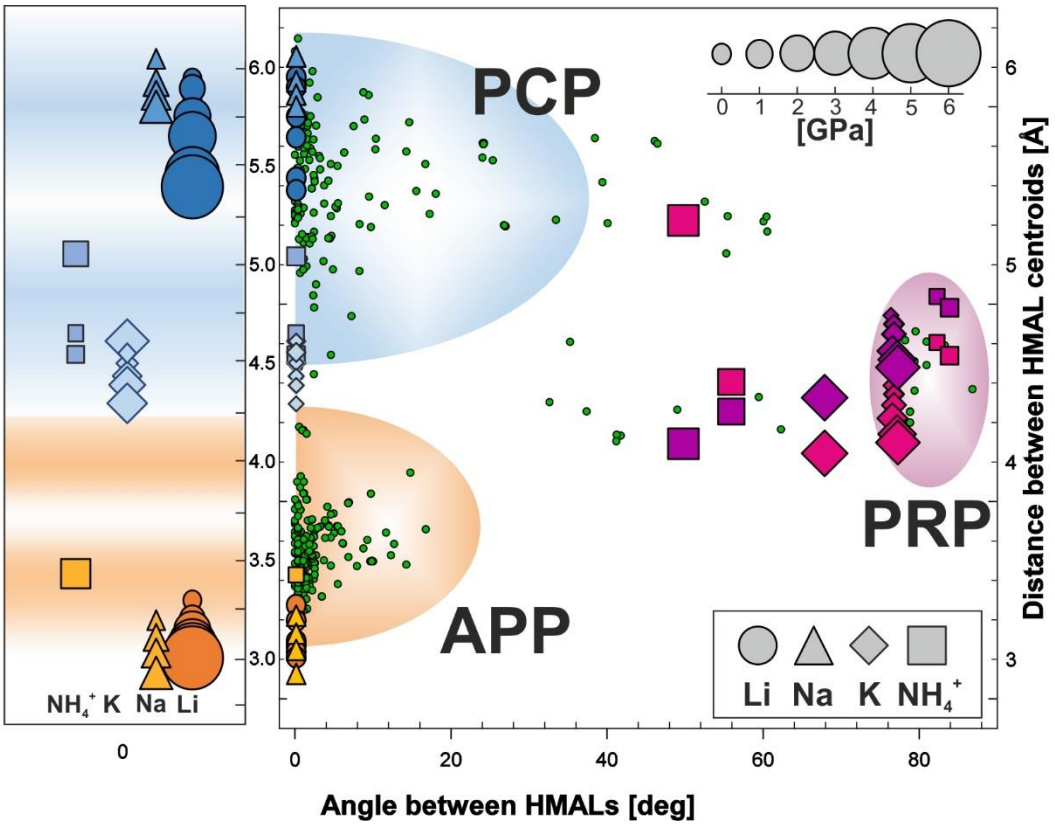

Figure 10. Evolution of the contact distances in different packing modes of HMAL under HP. Contacts evolution in the given geometry: violet- PRP (PRP1 and PRP2), blue - PCP, orange - APP. Green dots represent the entries from CSD (n = 208). Inset on the left: evolution of the contacts geometry between parallel HMALs ascribed to specific HMAL.

From a practical point of view, the performance of the studied HMALs at HP during formulation can be primarily judged by the pressure at which they undergo irreversible processes such as amorphization, as this may affect the kinetics of solvation, hence the bioavailability. Depending on size and shape of tablets, the achievable pressure in the rotary tableting machine can reach 1.2 GPa. while the typical operational pressure is typically in range 40-200 MPa[59,60]. Among the studied compounds, only LiHMAL remained crystalline within the studied pressure range up to 6.7 GPa, which coincides with the lowest compressibility among the HMALs group (Table 1).

Both, sodium and ammonium salts, despite different crystal packing, undergo amorphization already at around 2 GPa, and they present significantly higher compressibility than the other two compounds. KHMAL, while turning amorphous at twice the pressure of its ammonium analogue, shows a smaller compressibility and the highest pressure (3.77 GPa) of the first transition among the considered compounds. However, the occurrence of phase transitions and packing changes at HP is not a clue of the loss of crystallinity (Table 1). It seems that the presence of crystallization water does not play a major role in the stabilization of the crystal structure at HP, as NaHMAL, more hydrated than LIHMAL, turns into an amorphous phase at a pressure similar to the amorphization pressure of anhydrous NH4HMAL.

Table 1. Comparison of the various responses to HP in the studied compounds.

Compound	**Crystallization water**	**Phase transition pressure [GPa]**	**Change of coordination number**	**Amorphization pressure [GPa]**	**Estimated volume compression at 1.0 GPa**
LiHMAL	dihydrate	0.97(3)	4 → 6	n.a.	0.91
NaHMAL	trihydrate	n.a.	n.a.	> 1.93(3)	0.94
KHMAL	anhydrous	3.77(3)	6 → 8	> 4.01(3)	0.96
NH4HMAL	anhydrous	1.44(3)	6 → 9	> 2.06(3) a	0.91

Conclusions

The molecular response of HMAL salts of selected alkali metals and ammonium cations has been studied as a function of hydrostatic pressure. Collected results on the structural response for all of the studied compounds are presented in Figure 10 and Table 1. Structures with different

intermolecular motifs respond to pressure by increasing the coordination sphere around the cation, changing the HMAL packing or both.

The largest changes are experienced by structures, which exhibit in ambient condition a symmetric RAHB. With pressure, they experience shorter and more localized ionic contacts on one side of the molecule and a progressive destabilization of the PRP interactions between HMALs. In fact, at the highest pressure points, both in KHMAL (4.01 GPa) and NH4MAL (2.06 GPa) the heavy distortion leads to a phase transition to the lower symmetry, which destabilizes the RAHB from its initial position. In NH4MAL, moreover, there is change from PCP to APP conformation, which seems to be favored at high pressure as it distributes repulsive interactions on a larger volume. Despite being isostructural at ambient pressure, KHMAL and NH4HMAL response to pressure is different. The presence of the directional hydrogen bonds between counterions in NH4HMAL makes its structure more susceptible to a molecular rearrangement at HP. LiHMAL, with a less symmetric RAHB, responds to pressure mainly by the expansion of the coordination sphere around the Li atom from 4 to 6 oxygens and no further localization is experienced by the HMAL with respect to lateral cations. The small radius of the cation prevents the structure from further rearrangements through the steric hindrance between the enveloping oxygens. The species with the most localized RAHB, namely NaHMAL, is also the one with the least notable changes. It experiences a continuous compression in the axis perpendicular to the anion plane coupled with a formation of HMAL dimers in APP fashion, showing rigidity towards changes in the anion-cation interactions.

This study shows that at the hydrostatic pressure-range of circa 1 GPa, HMAL salts of small cations can undergo significant structural changes, sometimes associated with phase transitions. As the cation becomes bulkier and its interaction with HMAL becomes weaker, the onset of

structural changes, including amorphization occurs at lower pressure. It is particularly important in drug formulation and tableting where pressure up to 0.6 GPa [59,61,62] is applied on a HMAL compound with a bulky cation (such as in lisuride[8], tegaserod[63,64] or trimebutine HMAL[65]), particularly considering that such pressures are achieved in non-hydrostatic conditions, which favor irreversible processes. Unforeseen, HP-induced structural changes in such compounds may not only compromise the tablet integrity (e.g. through structural phase transitions), but more importantly its bioavailability (e.g. through amorphization) or even change in chemical properties (pressure-induced chemical reactions). Although the quality of the data and the undesired amorphization which occurs at HP did not allow higher pressure investigations, the observed structural alterations indicate a possible reactivity path between the carbonyl groups. Further studies should explore the influence of non-hydrostatic conditions, such as during the tableting, on the structural changes in HMALs, as well as spectroscopic studies on the amorphous phase. In fact, NH4HMAL was reported to react under HP non-hydrostatic conditions in the crystalline form and produce a mixture of amides, but the structural studies are still lacking [66].

Supporting information

The Supporting Information is available free of charge at .

Additional information on supramolecular conformations, Hirshfeld surface analysis, selected crystallographic and compressibility data for the studied compounds, details on the experimental conditions.

Acknowledgments

We thank the Swiss National Science Foundation (Project Nr. 162861 and NCCR Marvel) for the financial support.

References

(1) Stahl, P. H.; Wermuth, C. G. *Pharmaceutical Salts: Properties, Selection and Use*; John Wiley & Sons, 2002.

(2) Miller, G. Evaluation Of Two Tranquilizers: Acetophenazine Maleate (Tindal Maleate): Carphenazine Maleate (Proketazine Maleate. *JAMA* **1963**, *186*, 943–944.

(3) Burry, L.; Mehta, S.; Perreault, M. M.; Luxenberg, J. S.; Siddiqi, N.; Hutton, B.; Fergusson, D. A.; Bell, C.; Rose, L. Antipsychotics for Treatment of Delirium in Hospitalised Non-ICU Patients. *Cochrane Database of Systematic Reviews*. 2018. https://doi.org/10.1002/14651858.CD005594.pub3.

(4) Gál, G. T.; May, N. V.; Bombicz, P. Crystal Structure of Levomepromazine Maleate. *Acta Crystallogr. Sect. E Crystallogr. Commun.* **2016**, *72*, 612–615. https://doi.org/10.1107/S2056989016004916.

(5) Chlorphenamine Maleate. In *Meyler's Side Effects of Drugs*; Jeffrey K. Aronson, Ed.; Elsevier Science, 2016; p 270. https://doi.org/10.1016/b978-0-444-53717-1.00481-9.

(6) van Toor, B. S. J.; Buchwald, A.; Stengele, E.; Trenk, D.; Gercek, C.; de Mey, C. M. Systemic Bioavailability of Nasally Applied Chlorphenamine Maleate (0.4% Nasal Spray) Relative to Tablets Administered Perorally. *Int. J. Clin. Pharmacol. Ther.* **2001**, *39*, 173–178. https://doi.org/10.5414/cpp39173.

(7) Johnson, W. H.; Ireland, P. E. The Control of Vertigo by Thiethylperazine. *Arch. Otolaryngol.* **1965**, *82*, 261–266. https://doi.org/10.1001/archotol.1965.00760010263008.

(8) Ikoma, Y.; Hara, K.; Arita, S.; Oshino, N. Pharmacological Properties of Lisuride Hydrogen Maleate. Effects on the Central Nervous System. *Japanese Pharmacol. Ther.* **1982**, *10*,

125–136.

(9) Woo, H. K.; Wang, X. Bin; Wang, L. S.; Lau, K. C. Probing the Low-Barrier Hydrogen Bond in Hydrogen Maleate in the Gas Phase: A Photoelectron Spectroscopy and Ab Initio Study. *J. Phys. Chem. A* **2005**, *109*, 10633–10637. https://doi.org/10.1021/jp0553277.

(10) Zheng, Y. Q.; Kong, Z. P.; Lin, J. L. Refinement of the Crystal Structure of Sodium Hydrogen Maleate Trihydrate, NaH(C4H2O4) · 3H2O, at Room Temperature. *Zeitschrift fur Krist. - New Cryst. Struct.* **2001**, *216*, 377–378. https://doi.org/10.1524/ncrs.2001.216.14.377.

(11) Golic, L.; Leban, I. The Crystal Structure of Ammonium Hydrogen Maleate. *Croat. Chem. Acta* **1982**, *55*, 41–45.

(12) Darlow, S. F.; Cochran, W. The Crystal Structure of Potassium Hydrogen Maleate. *Acta Crystallogr.* **1961**, *14*, 1250–1257. https://doi.org/10.1107/s0365110x61003648.

(13) Popelier, P.; Lenstra, A. T. H.; Geise, H. J. Lithium Hydrogen Maleate Dihydrate. *Acta Crystallogr. Sect. C Cryst. Struct. Commun.* **1989**, *45*, 1024–1028. https://doi.org/10.1107/s0108270188014271.

(14) Flecka, M.; Bohatý, L. Syntheses, Crystal Structures and an Overview of Alkali Metal Maleates. *Zeitschrift fur Naturforsch. - Sect. B J. Chem. Sci.* **2009**, *64*, 517–524.

(15) Arkhipov, S. G.; Zakharov, B. A.; Boldyreva, E. V. Semi-Maleate Salts of <scp>L</Scp> - and <scp>DL</Scp> -Serinium: The First Example of Chiral and Racemic Serinium Salts with the Same Composition and Stoichiometry. *Acta Crystallogr. Sect. C Cryst. Struct. Commun.* **2013**, *69*, 517–521. https://doi.org/10.1107/S0108270113006720.

(16) Malaspina, L. A.; Edwards, A. J.; Woińska, M.; Jayatilaka, D.; Turner, M. J.; Price, J. R.; Herbst-Irmer, R.; Sugimoto, K.; Nishibori, E.; Grabowsky, S. Predicting the Position of the

Hydrogen Atom in the Short Intramolecular Hydrogen Bond of the Hydrogen Maleate Anion from Geometric Correlations. *Cryst. Growth Des.* **2017**, *17*, 3812–3825. https://doi.org/10.1021/acs.cgd.7b00390.

(17) Fillaux, F.; Leygue, N.; Tomkinson, J.; Cousson, A.; Paulus, W. Structure and Dynamics of the Symmetric Hydrogen Bond in Potassium Hydrogen Maleate: A Neutron Scattering Study. *Chem. Phys.* **1999**, *244*, 387–403. https://doi.org/10.1016/S0301-0104(99)00153-6.

(18) Olovsson, G.; Olovsson, I.; Lehmann, M. S. Neutron Diffraction Study of Sodium Hydrogen Maleate Trihydrate, NaH[C4H2O4].3H2O, at 120 K. *Acta Crystallogr. Sect. C Cryst. Struct. Commun.* **1984**, *40*, 1521–1526. https://doi.org/10.1107/s010827018400857x.

(19) Perrin, C. L.; Thoburn, J. D. Symmetries of Hydrogen Bonds in Monoanions of Dicarboxylic Acids. *J. Am. Chem. Soc.* **1992**, *114*, 8559–8565. https://doi.org/10.1021/ja00048a031.

(20) Avbelj, F.; Orel, B.; Klanjšek, M.; Hadži, D. Vibrational Spectra of Potassium Hydrogen Maleate Crystal and Solution. *Spectrochim. Acta Part A Mol. Spectrosc.* **1985**, *41*, 75–87. https://doi.org/10.1016/0584-8539(85)80087-8.

(21) Cardwell, H. M. E.; Dunitz, J. D.; Orgel, L. E. 764. The Structure of the Hydrogen Maleate Anion : A Symmetric Hydrogen Bond? *J. Chem. Soc.* **1953**, No. 0, 3740–3742. https://doi.org/10.1039/JR9530003740.

(22) Ríos, M. A.; Rodríguez, J. Ab Initio Study of the Structure of the Hydrogen Maleate Anion. *Can. J. Chem.* **1993**, *71*, 303–306. https://doi.org/10.1139/v93-044.

(23) McAllister, M. A. Characterization of Low-Barrier Hydrogen Bonds. 3. Hydrogen Maleate. An Ab Initio and DFT Investigation. *Can. J. Chem.* **2006**, *75*, 1195–1202.

https://doi.org/10.1139/v97-144.

(24) Garcia-Viloca, M.; González-Lafont, A.; Lluch, J. M. Theoretical Study of the Low-Barrier Hydrogen Bond in the Hydrogen Maleate Anion in the Gas Phase. Comparison with Normal Hydrogen Bonds. *J. Am. Chem. Soc.* **1997**, *119*, 1081–1086. https://doi.org/10.1021/ja962662n.

(25) Vener, M. V.; Manaev, A. V.; Hadzi, D.; Tsirelson, V. G. DFT Study of Proton Dynamics in the Potassium Hydrogen Maleate Crystal: The Infrared Versus the Inelastic Neutron Scattering Spectra. *Zeitschrift für Phys. Chemie* **2008**, *222*, 1349–1358. https://doi.org/10.1524/zpch.2008.5394.

(26) Vener, M. V.; Manaev, A. V.; Egorova, A. N.; Tsirelson, V. G. QTAIM Study of Strong H-Bonds with the O-H···A Fragment (A = O, N) in Three-Dimensional Periodical Crystals. *J. Phys. Chem. A* **2007**, *111*, 1155–1162. https://doi.org/10.1021/jp067057d.

(27) Vener, M. V.; Manaev, A. V.; Tsirelson, V. G. Proton Dynamics in Strong (Short) Intramolecular H-Bond. DFT Study of the KH Maleate Crystal. *J. Phys. Chem. A* **2008**, *112*, 13628–13632. https://doi.org/10.1021/jp806616q.

(28) Kawashima, Y.; Tachikawa, M. Ab Initio Path Integral Molecular Dynamics Study of the Nuclear Quantum Effect on Out-of-Plane Ring Deformation of Hydrogen Maleate Anion. *J. Chem. Theory Comput.* **2014**, *10*, 153–163. https://doi.org/10.1021/ct4007986.

(29) Schiott, B.; Iversen, B. B.; Madsen, G. K. H.; Larsen, F. K.; Bruice, T. C. On the Electronic Nature of Low-Barrier Hydrogen Bonds in Enzymatic Reactions. *Proc. Natl. Acad. Sci.* **2002**, *95*, 12799–12802. https://doi.org/10.1073/pnas.95.22.12799.

(30) Cleland, W. W.; Kreevoy, M. M. Low-Barrier Hydrogen Bonds and Enzymic Catalysis. *Science (80-.).* **1994**, *264*, 1887–1890. https://doi.org/10.1126/science.8009219.

(31) Gerlt, J. A.; Kreevoy, M. M.; Cleland, W. W.; Frey, P. A. Understanding Enzymic Catalysis: The Importance of Short, Strong Hydrogen Bonds. *Chemistry and Biology*. 1997, pp 259–267. https://doi.org/10.1016/S1074-5521(97)90069-7.

(32) Sobczyk, L.; Chudoba, D.; Tolstoy, P.; Filarowski, A. Some Brief Notes on Theoretical and Experimental Investigations of Intramolecular Hydrogen Bonding. *Molecules* **2016**, *21*, 1657. https://doi.org/10.3390/molecules21121657.

(33) Ritter, E.; Przybylski, P.; Brzezinski, B.; Bartl, F. Schiff Bases in Biological Systems. *Curr. Org. Chem.* **2009**, *13*, 241–249. https://doi.org/10.2174/138527209787314805.

(34) Schwartz, B.; Drueckhammer, D. G. A Simple Method for Determining the Relative Strengths of Normal and Low-Barrier Hydrogen Bonds in Solution: Implications to Enzyme Catalysis. *J. Am. Chem. Soc.* **1995**, *117*, 11902–11905. https://doi.org/10.1021/ja00153a011.

(35) Pan, Y.; McAllister, M. A. Characterization of Low-Barrier Hydrogen Bonds. 1. Microsolvation Effects. An Ab Initio and DFT Investigation. *J. Am. Chem. Soc.* **1997**, *119*, 7561–7566. https://doi.org/10.1021/ja9709684.

(36) Perrin, C. L.; Nielson, J. B. Asymmetry of Hydrogen Bonds in Solutions of Monoanions of Dicarboxylic Acids. *J. Am. Chem. Soc.* **1997**, *119*, 12734–12741. https://doi.org/10.1021/ja9729084.

(37) Groom, C. R.; Bruno, I. J.; Lightfoot, M. P.; Ward, S. C. The Cambridge Structural Database. *Acta Crystallogr. Sect. B Struct. Sci. Cryst. Eng. Mater.* **2016**, *72*, 171–179. https://doi.org/10.1107/S2052520616003954.

(38) Losev, E. A.; Zakharov, B. A.; Boldyreva, E. V. Polymorphic Transformations in Glycine Co-Crystals at Low Temperature and High Pressure: Two New Examples as a Follow-up to

a Glycine-Glutaric Acid Study. *CrystEngComm* **2016**, *18*, 5869–5875. https://doi.org/10.1039/c6ce00561f.

(39) Paliwoda, D.; Dziubek, K. F.; Katrusiak, A. Imidazole Hidden Polar Phase. *Cryst. Growth Des.* **2012**, *12*, 4302–4305. https://doi.org/10.1021/cg300852t.

(40) Zakharov, B. A.; Goryainov, S. V.; Boldyreva, E. V. Unusual Seeding Effect in the Liquid-Assisted High-Pressure Polymorphism of Chlorpropamide. *CrystEngComm* **2016**, *18*, 5423–5428. https://doi.org/10.1039/c6ce00711b.

(41) Giordano, N.; Beavers, C. M.; Kamenev, K. V.; Marshall, W. G.; Moggach, S. A.; Patterson, S. D.; Teat, S. J.; Warren, J. E.; Wood, P. A.; Parsons, S. High-Pressure Polymorphism in <scp>l</Scp> -Threonine between Ambient Pressure and 22 GPa. *CrystEngComm* **2019**, *21*, 4444–4456. https://doi.org/10.1039/C9CE00388F.

(42) Schettino, V.; Bini, R.; Ceppatelli, M.; Ciabini, L.; Citroni, M. Chemical Reactions at Very High Pressure. *ChemInform* **2005**, *36*. https://doi.org/10.1002/chin.200540276.

(43) Casati, N.; Macchi, P.; Sironi, A. Staggered to Eclipsed Conformational Rearrangement of [Co 2(CO)6(PPh3)2] in the Solid State: An X-Ray Diffraction Study at High Pressure and Low Temperature. *Angew. Chemie - Int. Ed.* **2005**, *44*, 7736–7739. https://doi.org/10.1002/anie.200502241.

(44) Merrill, L.; Bassett, W. A. Miniature Diamond Anvil Pressure Cell for Single Crystal X-Ray Diffraction Studies. *Rev. Sci. Instrum.* **1974**, *45*, 290–294. https://doi.org/10.1063/1.1686607.

(45) Klotz, S.; Chervin, J. C.; Munsch, P.; Le Marchand, G. Hydrostatic Limits of 11 Pressure Transmitting Media. *J. Phys. D. Appl. Phys.* **2009**, *42*.

(46) Forman, R. A.; Piermarini, G. J.; Barnett, J. D.; Block, S. Pressure Measurement Made by

the Utilization of Ruby Sharp-Line Luminescence. *Science (80-.).* **1972**, *176*, 284–285. https://doi.org/10.1126/science.176.4032.284.

(47) Willmott, P. R.; Meister, D.; Leake, S. J.; Lange, M.; Bergamaschi, A.; Böge, M.; Calvi, M.; Cancellieri, C.; Casati, N.; Cervellino, A.; Chen, Q.; David, C.; Flechsig, U.; Gozzo, F.; Henrich, B.; Jäggi-Spielmann, S.; Jakob, B.; Kalichava, I.; Karvinen, P.; Krempasky, J.; Lüdeke, A.; Lüscher, R.; Maag, S.; Quitmann, C.; Reinle-Schmitt, M. L.; Schmidt, T.; Schmitt, B.; Streun, A.; Vartiainen, I.; Vitins, M.; Wang, X.; Wullschleger, R. The Materials Science Beamline Upgrade at the Swiss Light Source. *J. Synchrotron Radiat.* **2013**, *20*, 667–682. https://doi.org/10.1107/S0909049513018475.

(48) Rigaku Oxford Diffraction Ltd, Yarnton, Oxfordshire, E. CrysAlis PRO. 2015.

(49) Farrugia, L. J. WinGX and ORTEP for Windows: An Update. *J. Appl. Crystallogr.* **2012**, *45*, 849–854. https://doi.org/10.1107/S0021889812029111.

(50) Sheldrick, G. M. SHELXT - Integrated Space-Group and Crystal-Structure Determination. *Acta Crystallogr. Sect. A Found. Crystallogr.* **2015**, *71*, 3–8. https://doi.org/10.1107/S2053273314026370.

(51) Sheldrick, G. M. Crystal Structure Refinement with SHELXL. *Acta Crystallogr. Sect. C Struct. Chem.* **2015**, *71*, 3–8. https://doi.org/10.1107/S2053229614024218.

(52) Dolomanov, O. V.; Bourhis, L. J.; Gildea, R. J.; Howard, J. A. K.; Puschmann, H. OLEX2: A Complete Structure Solution, Refinement and Analysis Program. *J. Appl. Crystallogr.* **2009**, *42*, 339–341. https://doi.org/10.1107/S0021889808042726.

(53) Viswanathan, M. High-Pressure Phase Transitions with Group–Subgroup Disagreement in Metal Guanidinium Formates. *CrystEngComm* **2018**, *20*, 6861–6866. https://doi.org/10.1039/C8CE01612G.

(54) Gupta, S. C.; Chidambaram, R. Symmetry Systematics of Pressure-Induced Phase Transitions. *High Press. Res.* **1994**, *12*, 51–70. https://doi.org/10.1080/08957959408203167.

(55) Olsher, U.; Izatt, R. M.; Bradshaw, J. S.; Dalley, N. K. Coordination Chemistry of Lithium Ion: A Crystal and Molecular Structure Review. *Chem. Rev.* **1991**, *91*, 137–164. https://doi.org/10.1021/cr00002a003.

(56) Torquato, S.; Jiao, Y. Dense Packings of Polyhedra: Platonic and Archimedean Solids. *Phys. Rev. E* **2009**, *80*. https://doi.org/10.1103/physreve.80.041104.

(57) Cliffe, M. J.; Goodwin, A. L. PASCal: A Principal Axis Strain Calculator for Thermal Expansion and Compressibility Determination. *J. Appl. Crystallogr.* **2012**, *45*, 1321–1329. https://doi.org/10.1107/S0021889812043026.

(58) Wilson, C. C.; Thomas, L. H.; Morrison, C. A. A Symmetric Hydrogen Bond Revisited: Potassium Hydrogen Maleate by Variable Temperature, Variable Pressure Neutron Diffraction and Plane-Wave DFT Methods. *Chem. Phys. Lett.* **2003**, *381*, 102–108. https://doi.org/10.1016/j.cplett.2003.09.055.

(59) Augsburger, L. L.; Hoag, S. W. Pharmaceutical Dosage Forms: Capsules. In *Pharmaceutical Dosage Forms: Capsules*; CRC Press, 2017; p 243. https://doi.org/10.1201/b19825.

(60) Thakral, N. K.; Thakral, S.; Stephenson, G. A.; Sedlock, R.; Suryanarayanan, R. Compression-Induced Polymorphic Transformation in Tablets: Role of Shear Stress and Development of Mitigation Strategies. *J. Pharm. Sci.* **2019**. https://doi.org/10.1016/j.xphs.2018.09.015.

(61) Matsumoto, R.; Kawakami, K.; Aoki, S. Impact of Compression Pressure on Tablet

Appearance. *Int. J. Pharm.* **2007**, *341*, 44–49. https://doi.org/10.1016/j.ijpharm.2007.03.055.

(62) Adeleye, O. A.; Femi-Oyewo, M. N.; Odeniyi, M. A. Effect of Compression Pressure on Mechanical and Release Properties of Tramadol Matrix Tablets. *Curr. Issues Pharm. Med. Sci.* **2015**, *28*, 120–125. https://doi.org/10.1515/cipms-2015-0057.

(63) Srivijaya, R.; Vishweshwar, P.; Sreekanth, B. R.; Vyas, K. Crystalline Forms and Aqueous Solubilities of an IBS Drug, Tegaserod. *CrystEngComm* **2008**, *10*, 283–287. https://doi.org/10.1039/b714374p.

(64) Cheng, Q.; Xu, X.; Liu, T.; Zhang, C. Tegaserod Maleate. *Acta Crystallogr. Sect. E Struct. Reports Online* **2007**, *63*. https://doi.org/10.1107/S1600536807047368.

(65) Iwata, T.; Uchida, M.; Takahashi, K.; Ogiwara, J.; Endoh, A.; Mori, T.; Hashimoto, Y.; Ohbayashi, S.; Saitoh, K.; Hondo, H.; Bando, K. Pharmacological Study of Trimebutine Maleate (I). Effect of Trimebutine Maleate on Gastric Motility in Rats. *Japanese Pharmacol. Ther.* **1992**, *20*, 349–359.

(66) Chistotina, N. P.; Zharov, A. A. Study of the Reactivity of Ammonium Carboxylates in the Synthesis of Amides under High-Pressure Deformation Conditions. *Bull. Acad. Sci. USSR Div. Chem. Sci.* **1989**. https://doi.org/10.1007/BF00962116.

For Table of Contents Use Only

On the structural variety of alkali hydrogen maleates at high pressure.

Tomasz Poręba, Piero Macchi, Nicola Casati

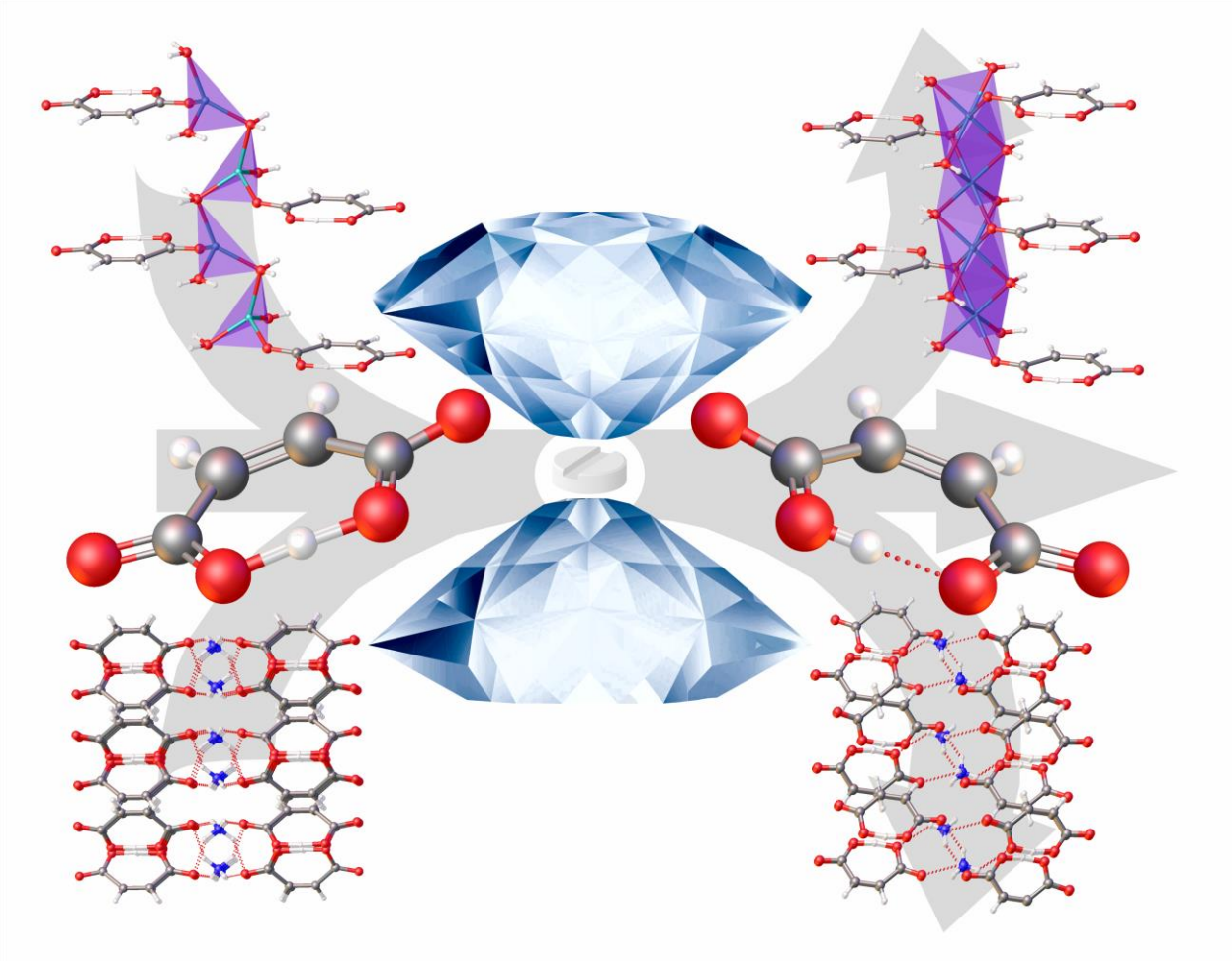

Alkali hydrogen maleates, show a multitude of structural responses upon load. Pressure-induced coordination increase, phase transitions and hydrogen-bonding alteration may affect the physical properties of these salts, as well as their performance in pharmaceutical formulations.